Use of Multi-Resolution Imager Data to Account for Partially Cloud-Filled Pixels

L. Nguyen, P. Minnis, D. V. Young, and W. L. Smith Jr.
Atmospheric Sciences
National Aeronautics Space Administration
Langley Research Center
Hampton, Virginia

P. W. Heck, A. D. Rapp, and M. M. Khaiyer
Analytical Services and Materials, Inc.
Hampton, Virginia

Introduction

Partially cloud-filled pixels are a significant problem for satellite remote sensing of cloud properties. Optical depths and effective particle sizes are often too small or too large, respectively, when derived from radiances that are assumed to be overcast but contain radiation from both clear and cloud areas within the satellite imager field of view. This has been demonstrated most recently by Dong et al. (2002), which compared surface and satellite retrievals over the Atmospheric Radiation Measurement (ARM) Program's Southern Great Plains (SGP) Central Facility (CF). For example, the breakup of a solid cloud deck caused a rapid divergence of the two retrieved cloud droplet sizes in one of their case studies. This effect is important because it biases the statistics of the cloud properties being generated for ARM over all surface sites. Minimization of the effect is necessary to increase the accuracy of the ARM satellite cloud products.

The remote sensing problems that arise are due to two effects: the underestimate of cloud fraction in the pixel and the deviation of the reflectance behavior from the plane-parallel cloud assumption used in the retrieval models. While the latter is relatively intractable, the former can be addressed by estimating the cloud fraction within each pixel. The nominal resolution for most channels on the Geostationary Operational Environmental Satellite (GOES) imager is 4 km, but the GOES imager also takes visible (VIS, 0.65 μm) channel data at 1 km. Thus, it should be possible to obtain an improved estimate of cloud fraction within the lower resolution pixels by using the information contained in the higher resolution VIS data. This paper explores the use of multi-resolution datasets to determine if the additional information can be used successfully to reduce the effect of partially cloud-filled pixels on retrieved cloud properties.

Methodology and Data

Minnis et al. (2002) describe the Visible Infrared Solar-infrared Split-window Technique (VISST) that uses the visible (VIS; 0.65 μm), infrared (IR; 10.8 μm), solar infrared (SIR; 3.9 μm) and split-window

infrared (12.0 μm) channel to derive cloud height; phase; optical depth; effective particle size, either ice crystal diameter D_e or droplet radius r_e; and either liquid water path (LWP) or ice water path (IWP) for each GOES-8 pixel determined to be cloudy. The cloud mask (CM) (Trepte et al. 1999) consists of a decision tree, illustrated schematically in Figure 1, that compares the observed VIS, IR, and SIR radiances with a set of thresholds based on the a priori estimates of the clear VIS reflectance, the skin temperature, the surface emissivities, the vertical profile of temperature and water vapor, and the variation of these values within a 0.5° box. A consistent value of clear or cloudy in all three channels results in an immediate classification of the pixel as clear or cloudy. Otherwise, a series of additional tests, "C tests," are performed to classify the pixel. If it is cloudy, then the observed radiances are used in the VISST to derive the cloud properties.

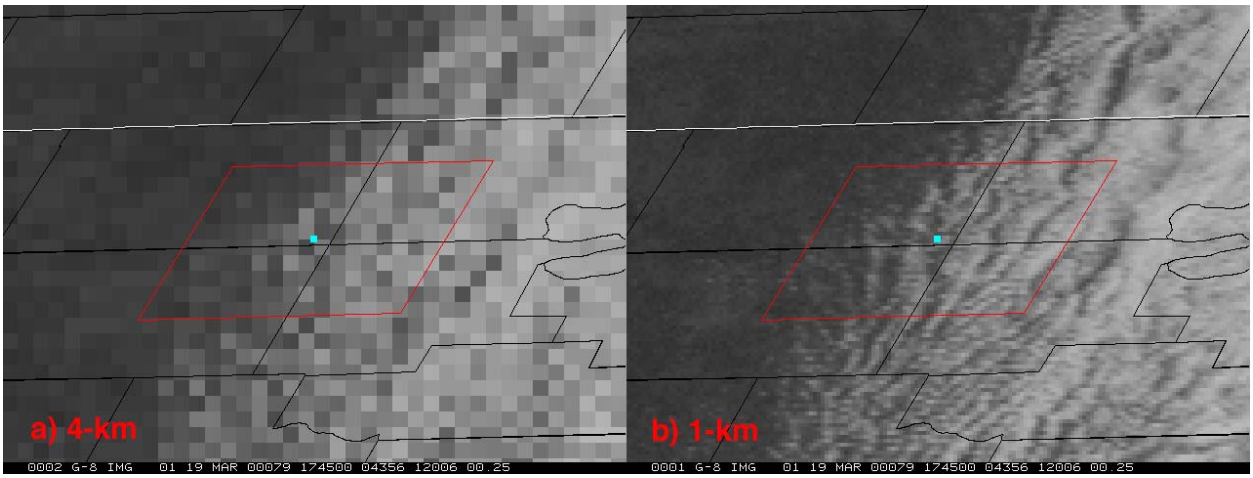

Figure 1. GOES-8 multi-spectral cloud mask for VISST.

The nominal 4-km VIS data are actually sampled 1-km VIS radiances. Thus, to use the 1-km pixels P_1, the 4 x 4 array of 1-km pixels that matches the 4-km pixels P4 must first be determined. This is accomplished by computing the average reflectance for a series of 4 x 4 arrays created by shifting the starting line or element of the array within the image. These pixels are then assigned to the nearest IR pixel and a set of the matched VIS and IR pixels are correlated. The shifts in starting line and element corresponding to the highest correlation are then used to create a new averaged 4-km VIS reflectance and an array of 16 1-km VIS reflectances that are linked to a particular set of IR line and element coordinates. The line and element shifts for the 1-km data vary by 1 or 2 positions from image to image.

This new dataset is then analyzed with the CM to determine which 4-km pixels are cloudy. If the CM(P_4) is cloudy, then the 1-km data are tested using a simple VIS reflectance threshold. If the reflectance exceeds the threshold, then the 1-km pixel is cloudy. The ratio of the cloudy 1-km pixels to 16 constitutes the cloud fraction C_4 for P_4. The value of C_4 is then sent to VISST, which computes the top-of-atmosphere radiance for each cloud model and wavelength as

$$R(C_4) = (1 - C_4)R_{cs} + C_4\ R(\text{cloud model}),$$

where R_{cs} is the clear-sky radiance for the particular channel. These calculated model values are then compared with the observed radiances to retrieve the cloud properties.

In this initial study, a fixed VIS threshold is used to test each P_1 over a 400 x 400 km region centered on the CF. Half-hourly GOES-8 data taken between 1200 and 2345 Universal Time Coordinates (UTC) March 19, 2000, are analyzed using the P_4 data alone and then the P_1 data. Examples of the matched 4 and 1-km images are shown in Figure 2 for 1745 UTC. The clouds are situated at approximately 1.5 km above the surface and marked by gaps that are primarily oriented along the north-south direction and by some smaller scale cellular structure evident in Figure 2b. The cloud deck was moving from west to east during the day with the structure in Figure 2 passing over the CF after 1600 UTC. Otherwise, the clouds were unbroken. Figure 3 shows a comparison of the cloud fractions derived from the surface using CM(P_4), the Whole-Sky Imager (WSI), and the ARM active remote sensing of clouds (ARSCL) product (Clothiaux et al. 2000). Except for 1400 to 1700 UTC, when it is close to the ARSCL results, the CM(P_4) tracks fairly closely with the WSI. Between 1900 and 2000 UTC, CM(P_4) yields less cloud coverage than either instrument.

Results

Figure 4 shows an example of the values of r_e derived for the P_4 and P_1 datasets at 1745 and 1945 UTC. Along the western edge of the cloud deck, r_e increases westward from about 10 μm to over 18 μm at 1745 UTC (Figure 4a). By computing the cloud fraction for each pixel, r_e rarely exceeds 12 μm in the same strip along the edge of the cloud deck, except for the southern fourth of the area where little change is evident between the 4- and 1-km results. Apparently, in that area, the single-value threshold used for detecting clouds in the 1-km VIS data was too low and detected few 4-km pixels with $C_4 < 1$. The results for 1945 UTC (Figure 4b) are similar with few values exceeding 10 μm for the 1-km results. The droplet sizes for the scattered clouds west of the cloud deck in Figure 4b decrease substantially when CM(P_1) is applied. The results in Figure 4 are typical for the day.

The average P_1 and P_4 values of r_e and LWP for a 0.5° box centered on the SCF are plotted in Figure 5 with the results from Dong et al. (2002) that are based on surface radar and radiometer data. The mean effective radii from the satellite data diverge dramatically from the surface data beginning at 1600 UTC reaching values up 17 μm. The new P_1 results yield a maximum mean r_e of 12 μm, a value much closer to the peak derived from the surface data. LWP(P_1) decreased relative to LWP(P_4) for all hours except at 1745 UTC when it rose slightly above the low-resolution result. These lower values are closer to those derived from the surface observations. The optical depths increased slightly but not enough to offset the decreases in r_e resulting in a general decrease in LWP. Figure 6 demonstrates how the value of r_e decreased as a function of the original optical depth $\tau(P_4)$. The greatest changes occurred for the smaller optical depths indicating that the broken clouds along the edge of the deck were broken rather than optically thin.

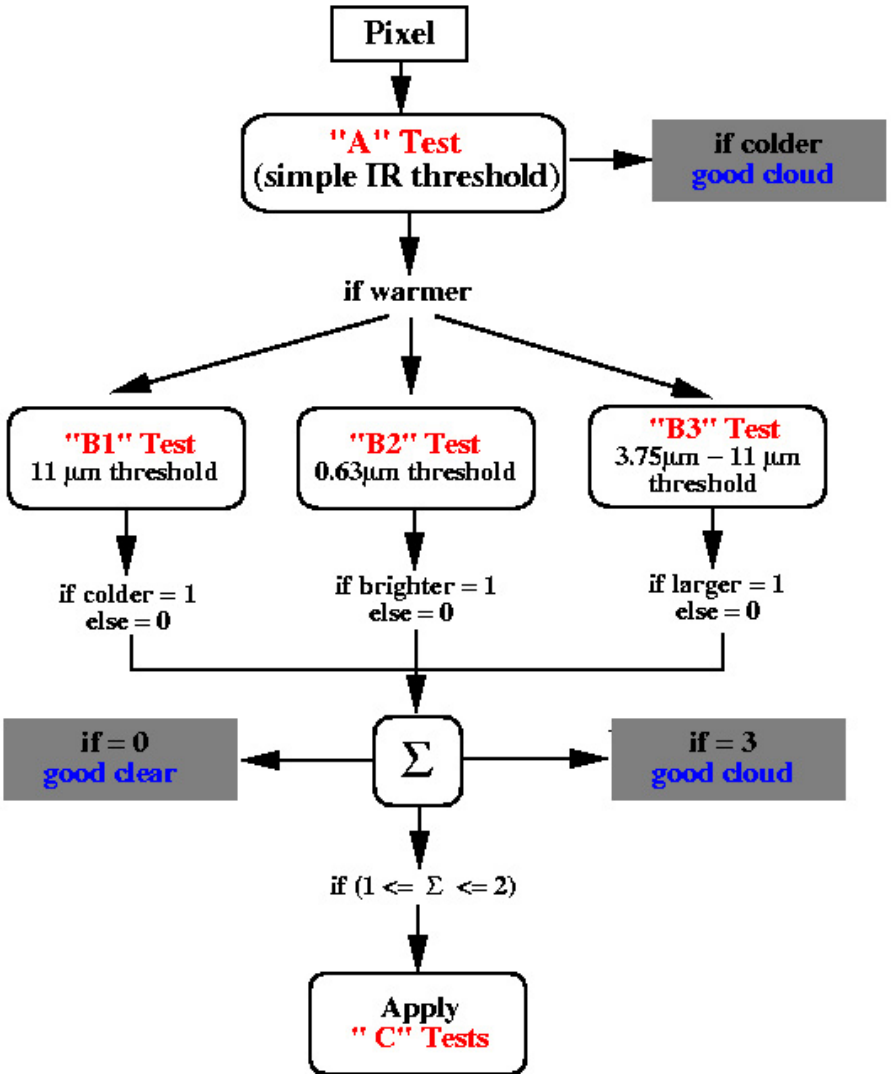

Figure 2. GOES-8 visible images over ARM SGP CF taken at 1745 UTC March 19, 2000.

Discussion

This initial case clearly demonstrates that incorporation of higher resolution data, even when only one channel is available, yields more reasonable cloud properties than obtained with low-resolution data only. However, much additional research is required before this type of approach can be implemented operationally. The assumption that a simple VIS threshold can discriminate between thin and broken clouds is valid only as long as the clouds in the larger pixel are thick enough to produce a significant VIS reflectance. Thin cirrus clouds are often nearly transparent at VIS wavelengths. Therefore, this approach should not be applied to cirrus clouds or the VIS threshold should be adjusted for the type of cloud in the pixel. One means for classifying each pixel as cirrus or otherwise would be to retain for each P_4 the classification of low, middle, or high cloud that is assigned each pixel in the layer bispectral threshold method (Minnis et al. 1995), the algorithm that serves as the initial step in the VISST.

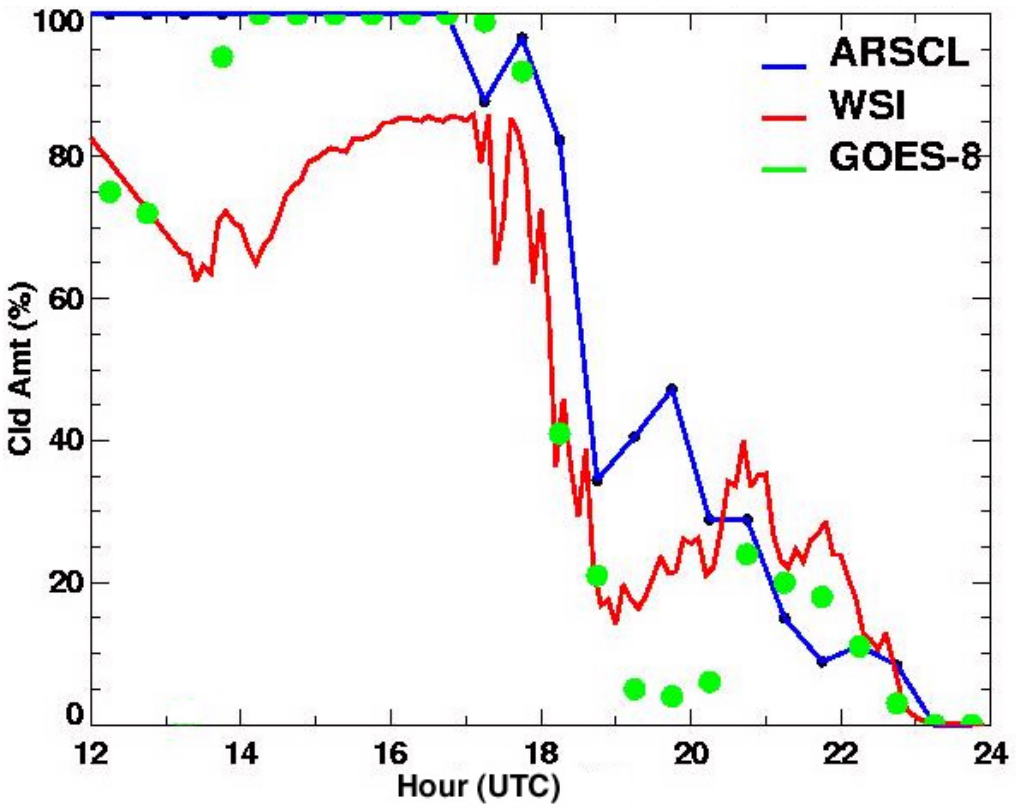

Figure 3. Time series of surface-based and GOES-8 cloud amounts, March 19, 2000.

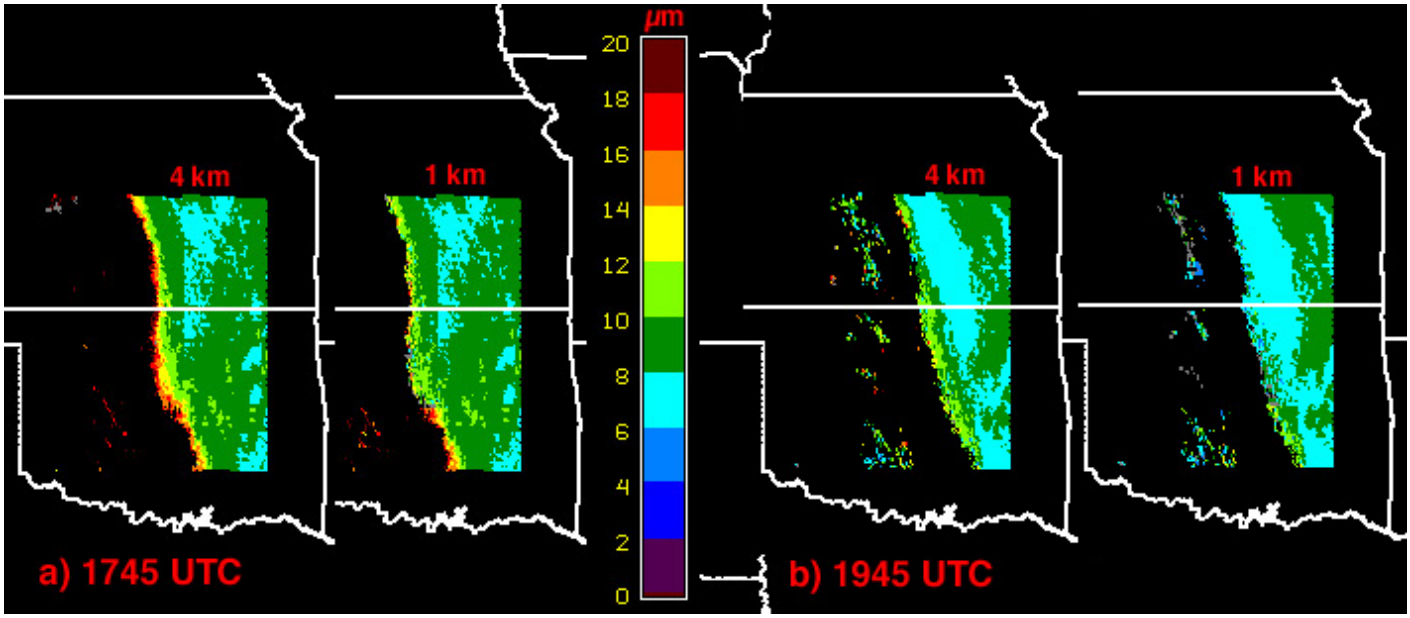

Figure 4. Cloud effective droplet radius from VISST, March 19, 2000.

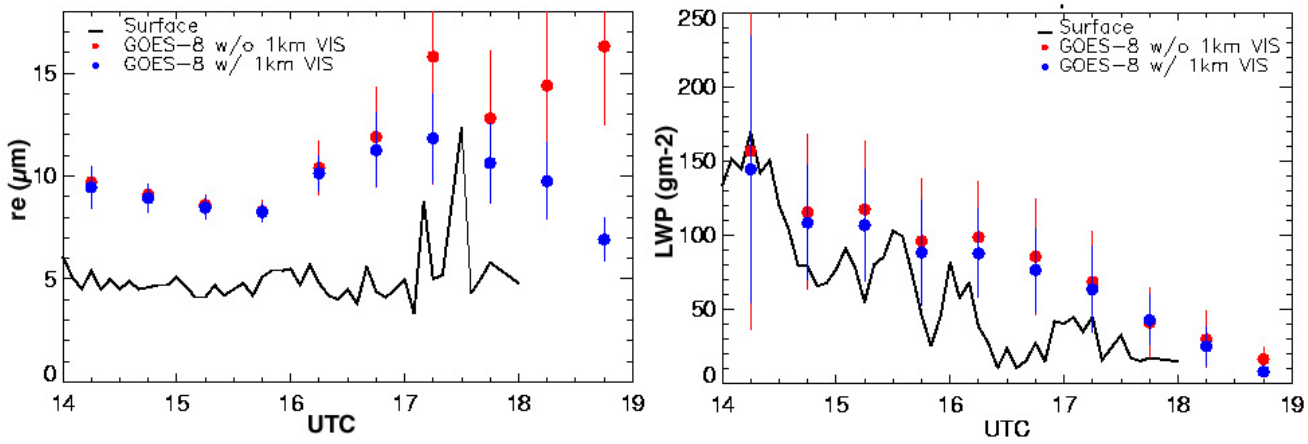

Figure 5. Comparison of cloud properties from the surface and 4 and 1-km GOES-8 data.

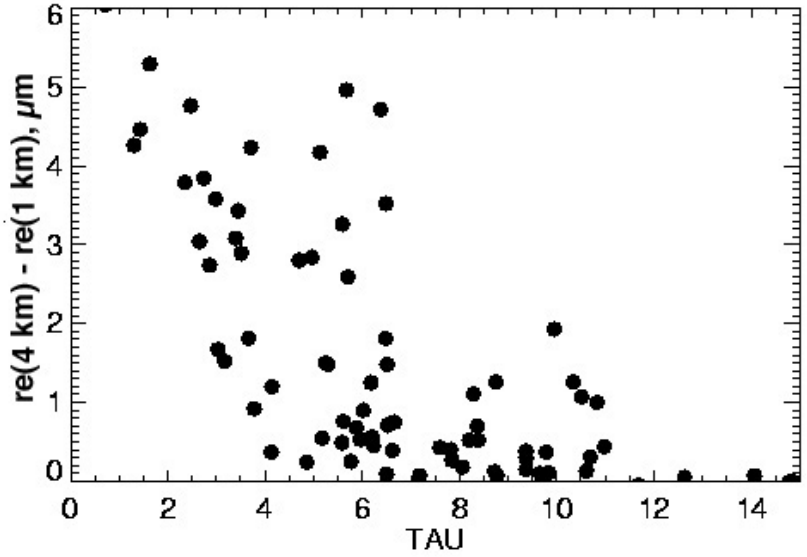

Figure 6. Decrease in r_e as a function of $\tau(P_4)$.

One scenario for applying the 1-km enhancement method would be to select only low and midlevel clouds first. Then, a test for adjacent clouds could be used to determine those pixels that are on the edge of a cloud field. In the case of edge pixels, it may be possible to apply the technique to cirrus clouds to prevent an overestimate of D_e or an underestimate of τ. Other approaches for implementing this method are certainly possible.

It is clear from Figure 4 that the local clear-sky reflectance and, hence, the 1-km VIS threshold should be characterized more accurately. Otherwise, large errors in the cloud fraction may result with subsequent errors in the derived properties. In this study, the cloud fraction was only computed for P_4's that had been classified as cloudy. However, there are probably pixels that are classified as clear that contain small amounts of clouds. Therefore, the criteria for computing sub-pixel fractional cloudiness should be expanded such that many of these smaller cloud amounts can be taken into account.

Concluding Remarks and Future Research

The use of multi-resolution data for alleviating some of the errors in cloud property retrievals appears to be promising, at least for low and midlevel clouds. The approach does not account for the three-dimensional structure of the clouds and its effect on the radiances, which are assumed to come from plane-parallel clouds. That effect is likely to increase as the subpixel cloud fraction decreases. The method used here requires careful alignment of the 4 and 1-km pixels, a task that can be CPU-intensive because the alignment appears to change slightly with each image.

This method should be applicable to any set of multi-resolution data including the Moderate-resolution Imaging Spectroradiometer (MODIS) on the Terra satellite. Its application will require higher resolution maps of clear-sky reflectance than are currently used. Using such maps necessitates very accurate navigation of each imager pixel. The proper VIS thresholds for accurately detecting the subpixel clouds must also be established. The process will probably require thresholds that depend on the solar zenith angle and the background reflectance.

Finally, it should be noted that only one cloud case was examined here, so it is essential that many different cloud conditions should be tested with this approach before it can be implemented in any operational scheme. Such testing will use both multi-resolution data like GOES and MODIS, but will also involve the creation of artificial 4-km pixels from 1-km pixels that have radiances at all wavelengths.

Corresponding Author

L. Nguyen, l.nguyen@larc.nasa.gov, (757) 864-5671

References

Clothiaux, E. E., T. P. Ackerman, G. G. Mace, K. P. Moran, R. T. Marchand, M. Miller, and B. E. Martner, 2000: Objective determination of cloud heights and radar reflectivities using a combination of active remote sensors at the ARM CART sites. *J. Appl. Meteorol.*, **39**, 645-665.

Dong, X., P. Minnis, G. G. Mace, W. L. Smith Jr, M. Poellot, and R. Marchand, 2002: Comparison of stratus cloud properties deduced from surface, GOES, and aircraft data during the March 2000 ARM Cloud IOP. *J. Atmos. Sci.*, accepted.

Minnis P., W. L. Smith, Jr., D. F. Young, L. Nguyen, A. D. Rapp, P. W. Heck, and M. M. Khaiyer, 2002: Near-real time retrieval of cloud properties over the ARM CART area from GOES data. This Proceedings.

Minnis P., W. L. Smith, Jr., D. P. Garber, J. K. Ayers, and D. R. Doelling, 1995: "Cloud properties derived from GOES-7 for Spring 1984 ARM Intensive Observing Period using Version 1.0.0 of ARM satellite data analysis program." *NASA RP 1366*, p. 58.

Trepte, Q., Y. Chen, S. Sun-Mack, P. Minnis, D. F. Young, B. A. Baum, and P. W. Heck, 1999: Scene identification for the CERES cloud analysis subsystem. *Proc. AMS 10th Conf. Atmos. Rad.*, June 28–July 2, 1999, 169-172, Madison, Wisconsin.